Article

Neuron

Coordinated Reductions in Excitatory Input to the Nucleus Accumbens Underlie Food Consumption

Highlights

- Rostral and caudal NAc have distinct inputs with divergent feeding-related activity
- Consumption coincides with a synchronous dip in excitatory input to the rostral NAc
- Reduced excitatory input to the NAc shell from multiple sources promotes feeding
- Excitatory inputs to the NAc contain heterogeneous activity during reward seeking

Authors

Sean J. Reed, Christopher K. Lafferty, Jesse A. Mendoza, ..., Logan Grosenick, Karl Deisseroth, Jonathan P. Britt

Correspondence

jonathan.britt@mcgill.ca

In Brief

Reed et al. report that opposing activity is present within each of the excitatory afferents to the nucleus accumbens during reward-seeking behavior. Synchronized reductions in excitatory input to the rostral nucleus accumbens shell correlate with and promote food consumption.

Reed et al., 2018, Neuron *99*, 1260–1273
September 19, 2018
https://doi.org/10.1016/j.neuron.2018.07.051

CellPress

CellPress

Neuron
Article

Coordinated Reductions in Excitatory Input to the Nucleus Accumbens Underlie Food Consumption

Sean J. Reed,[1] Christopher K. Lafferty,[2] Jesse A. Mendoza,[2] Angela K. Yang,[1] Thomas J. Davidson,[3] Logan Grosenick,[4] Karl Deisseroth,[5] and Jonathan P. Britt[1,2,6,7,*]

[1]Integrated Program in Neuroscience, McGill University, Montreal, QC, Canada
[2]Department of Psychology, McGill University, Montreal, QC, Canada
[3]Department of Physiology and Kavli Institute for Fundamental Neuroscience, University of California, San Francisco, San Francisco, CA, USA
[4]Department of Statistics, Columbia University Medical Center, New York, NY, USA
[5]Department of Bioengineering, Stanford University, Stanford, CA, USA
[6]Center for Studies in Behavioral Neurobiology, Concordia University, Montreal, QC, Canada
[7]Lead Contact
*Correspondence: jonathan.britt@mcgill.ca
https://doi.org/10.1016/j.neuron.2018.07.051

SUMMARY

Reward-seeking behavior is regulated by a diverse collection of inputs to the nucleus accumbens (NAc). The information encoded in each excitatory afferent to the NAc is unknown, in part because it is unclear when these pathways are active in relation to behavior. Here we compare the activity profiles of amygdala, hippocampal, and thalamic inputs to the NAc shell in mice performing a cued reward-seeking task using GCaMP-based fiber photometry. We find that the rostral and caudal ends of the NAc shell are innervated by distinct but intermingled populations of forebrain neurons that exhibit divergent feeding-related activity. In the rostral NAc shell, a coordinated network-wide reduction in excitatory drive correlates with feeding, and reduced input from individual pathways is sufficient to promote it. Overall, the data suggest that pathway-specific input activity at a population level may vary more across the NAc than between pathways.

INTRODUCTION

The nucleus accumbens (NAc) is a forebrain structure that regulates the likelihood of animals engaging in reward-seeking behavior and consuming food (Floresco, 2015; Nicola, 2007; Richard et al., 2013; Salamone et al., 2007). Presentation of reward-associated stimuli influences spiking activity in the NAc in a manner that reflects the value of the cue (du Hoffmann and Nicola, 2014; Nicola et al., 2004a), the animal's proximity to the reward (McGinty et al., 2013; Morrison and Nicola, 2014), and the likelihood of the animal seeking out the reward at that moment (Morrison et al., 2017; Sugam et al., 2014). This activity in the NAc is driven by excitatory inputs from a variety of forebrain regions, including the amygdala, hippocampus, thalamus, and prefrontal cortex (Ambroggi et al., 2008; Bagot et al., 2015; Britt et al., 2012; Do-Monte et al., 2017; Haight et al., 2017). These inputs likely encode the value of stimuli and action plans in a context-dependent manner (Mannella et al., 2013), but it is unclear what particular information is encoded in each input because it is largely unknown when each pathway is active relative to behavior. Probing this network activity during natural behavior may provide insight into how maladaptive circuit adaptations contribute to unhealthy behavior. Abnormal NAc physiology has been associated with several psychiatric conditions, including depression (Bagot et al., 2015; Francis and Lobo, 2017), addiction (Britt and Bonci, 2013; Volkow and Morales, 2015), eating disorders (Avena and Bocarsly, 2012), and schizophrenia (Chambers et al., 2001; Floresco et al., 2009).

During reward-seeking tasks, spiking activity in the NAc is highly variable across neurons (Guillem et al., 2014; Morrison et al., 2017; Nicola et al., 2004a, 2004b; West and Carelli, 2016). For instance, some NAc neurons show transient excitations when animals are presented with reward-associated cues, whereas others show sustained reductions in spiking activity that last throughout the period of reward consumption (Krause et al., 2010; Morrison et al., 2017; Nicola et al., 2004a, 2004b). This divergent activity may reflect variability in NAc neuron excitability in combination with local circuit dynamics (Cacciapaglia et al., 2011; Chuhma et al., 2011; Dobbs et al., 2016; Pennartz et al., 1994; Taverna et al., 2004). It may also relate to variations in afferent input, in part because of pathway-specific differences in innervation patterns and activity (Ambroggi et al., 2008; Ishikawa et al., 2008b; Jones et al., 2010). It is presently unknown whether any of the pathway-defined afferents to the NAc have distinctive activity patterns at a population level, although the inputs are associated with distinct cognitive processes (Floresco, 2015; Humphries and Prescott, 2010). Neural activity has been recorded in forebrain regions upstream of the NAc during reward-seeking tasks, but there is variable activity among neurons in those areas as well (Ambroggi et al., 2008; Ciocchi et al., 2015; Do-Monte et al., 2017; Kim et al., 2017; Li et al., 2016; Otis et al., 2017; Tye et al., 2010).

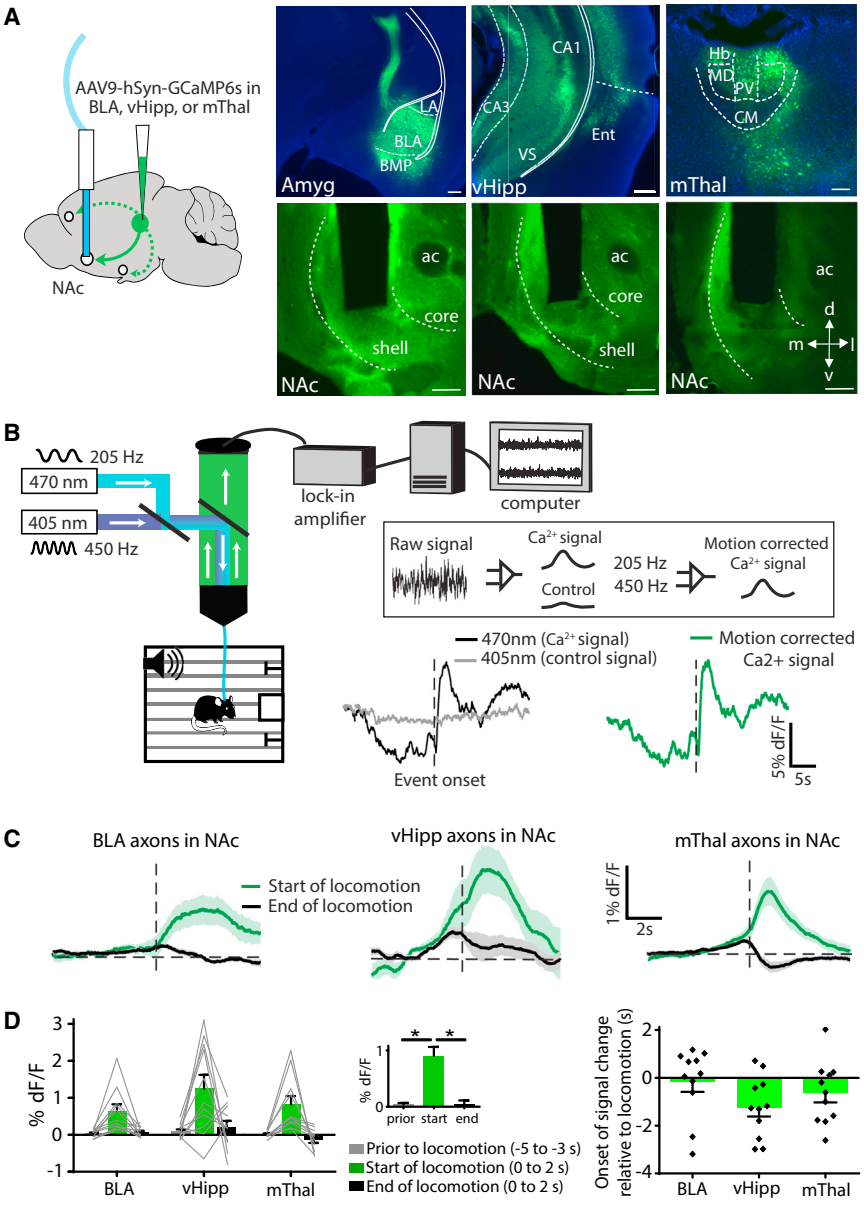

Figure 1. Onset of Locomotion Correlates with Increased Excitatory Input to the NAc Shell

(A) Schematic of optic probe placement in the NAc shell of a mouse infected with AAV9-hSyn-GCaMP6s in the BLA, vHipp, or mThal (left). Coronal brain slices from representative mice show GCaMP fluorescence at the injection site and in the NAc (right). LA, lateral amygdala; BLA, basolateral amygdala; BMP, basomedial posterior amygdala; VS, ventral subiculum; Ent, entorhinal cortex; Hb, habenula, MD, mediodorsal; PV, paraventricular, CM, central medial; ac, anterior commissure; v, ventral; m, medial; l, lateral; d, dorsal. Scale bars, 200 μm.

(B) Schematic of fiber photometry setup and signal processing. Light directed into the NAc varied in intensity in a sinusoidal pattern (470 nm at 205 Hz and 405 nm at 450 Hz). Fluctuations in the intensity of 530-nm light emitted from the brain were demodulated into calcium-sensitive GCaMP fluorescence (205 Hz) and non-neuronal artifact (450 Hz). The latter was scaled to best fit the calcium-sensitive signal and then subtracted from it to produce a motion-corrected signal.

(C) Average change in pathway-specific GCaMP6s fluorescence for three different inputs to the NAc shell in relation to the start and end of exploratory locomotor movements. Shaded areas represent SEM.

(D) Summary of the amplitude (signal mean in 2-s window) and timing of input activity in relation to locomotion. The inset highlights the shared change in input activity. Onset times are when the signal deviated from its baseline mean by more than 2 SDs. **$p < 0.05$, Sidak post hoc tests. Error bars represent SEM.

Evidence of population-level differences in pathway-defined inputs to the NAc would provide insight into the information each pathway encodes as well as NAc information processing in general. Accordingly, we sought to compare the activity of several prominent excitatory inputs to the NAc in mice performing a discriminative stimulus operant reward-seeking task. We report that pathway-defined input activity at a population level varies more across the NAc shell than between pathways, at least in relation to food port visits and reward consumption. In part, this is because the rostral and caudal ends of the NAc shell receive divergent input activity that arises from distinct but intermingled populations of upstream neurons. In the rostral NAc shell, a coordinated reduction in input activity across multiple pathways correlates with and drives food consumption.

RESULTS

To identify when pathway-defined inputs to the NAc shell are active in relation to behavior, we targeted expression of GCaMP6s (Chen et al., 2013) to areas of the forebrain that contain NAc-projecting neurons and, 1 month later, recorded axonal GCaMP fluorescence from the NAc shell (Figure 1A). Across mice, appreciable GCaMP signals were evident in projections from the basolateral amygdala (BLA), ventral hippocampus (vHipp), and midline thalamus (mThal). There was insufficient signal from prefrontal cortex input, so this afferent was not explored in this manner.

To control for any changes in fluorescence unrelated to neural activity, we simultaneously recorded calcium-sensitive and insensitive GCaMP fluorescence using 470-nm and 405-nm light, respectively (Figure 1B; Kim et al., 2016; Muir et al., 2017). We subtracted the calcium-insensitive isosbestic signal from the calcium-sensitive signal after scaling it to fit using least-squares regression (Kim et al., 2016; Muir et al., 2017). The resultant motion-corrected calcium signal was divided by its mean value to obtain the fractional fluorescence response (dF/F).

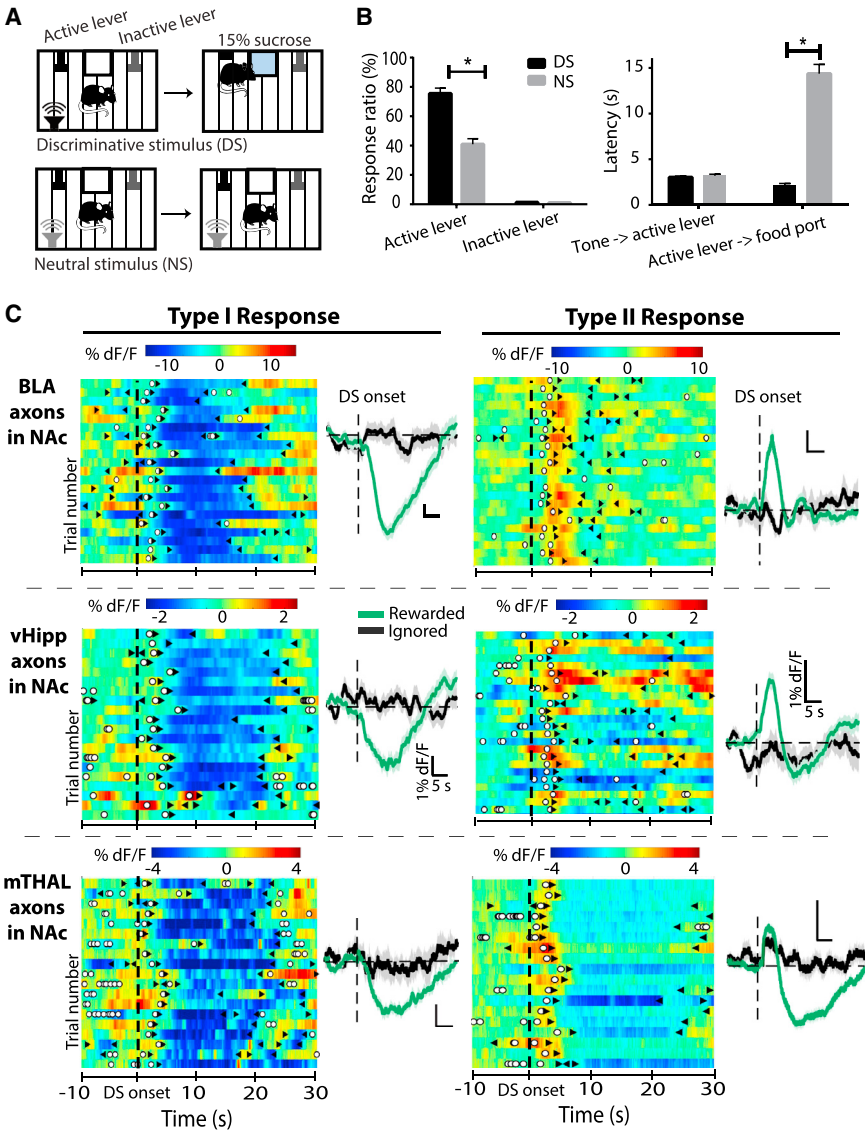

Figure 2. Divergent Activity Is Present within Each Afferent Pathway during Reward Delivery

(A) Schematic of the behavioral task. The first active lever press during each DS presentation triggered reward delivery.

(B) Summary of task performance and behavioral response latencies. The response ratio is the proportion of stimulus presentations that elicited a lever press response. Error bars represent SEM. *$p < 0.05$.

(C) Representative single-session data from 6 mice showing pathway-specific activity aligned to DS presentations. The two examples of each pathway (type 1 and type 2) emphasize the variability between mice and similarities across pathways. Color plots show changes in pathway-specific GCaMP fluorescence across every rewarded trial (open circles indicate lever presses; triangles bracket food port visits). Line graphs highlight the difference in activity between rewarded and ignored DS presentations. Scale bars, 1% dF/F, 5 s. Shaded areas of line graphs represent SEM.

Input-Specific Activity Is Evident in Each Pathway during Periods of Reward Obtainment

Because the amygdala, hippocampus, and thalamus contribute very differently to behavior, we hypothesized that their projections would have distinct activity patterns when mice had specific reasons to exhibit or withhold particular behaviors. Accordingly, we trained the mice on a discriminative stimulus operant reward-seeking task that has been repeatedly used to study NAc function (Ambroggi et al., 2008; du Hoffmann and Nicola, 2014; Ishikawa et al., 2008b; Nicola et al., 2004a; Yun et al., 2004b). In this task, one of two tones, either a discriminative stimulus (DS) or a non-rewarded stimulus (NS), each 10 s long, is presented every minute on average, and food delivery is coupled to the first active lever press made during each DS presentation (Figure 2A).

Previous studies of rats performing this task have found that the amount of lever pressing, food port visits, and rewards earned are all sensitive to pharmacological manipulations that disrupt glutamate or dopamine signaling in the NAc (Ambroggi et al., 2008, 2011; du Hoffmann and Nicola, 2014; Yun et al., 2004a). Another reason for the popularity of this task is that noisy neurophysiological recordings can be aligned to a variety of discrete behavioral events that occur repeatedly during a single session, which makes it possible to isolate the average change in neural activity that coincides with these behaviors (Ambroggi et al., 2008; Nicola et al., 2004a).

Pathway-specific measurements of axonal GCaMP6s fluorescence were collected over several sessions after task

Locomotor Movements Correlate with Increased Excitatory Input to the NAc Shell

The NAc is known to regulate certain kinds of approach behavior (Morrison and Nicola, 2014; Nicola, 2016), so to assess the feasibility of using fiber photometry to measure NAc excitatory input, we first aligned GCaMP fluorescence with animals' locomotion in an activity box (Figure 1C; n = 11 per pathway). The start but not the end of exploratory locomotor movements coincided with increases in axonal fluorescence in each of the examined inputs (Figure 1D; 2-way ANOVA; main effect of time, $F_{(2,60)} = 21.49$, $p < 0.001$, but not pathway; no interaction effect, $F_{(4,60)} = 0.77$, $p = 0.55$). The onset of these signal changes generally preceded the start of locomotion and did not differ significantly between pathways (Figure 1D; 1-way ANOVA, $F_{(2,30)} = 1.78$, $p = 0.19$). These data are consistent with the idea that excitatory input to the NAc promotes locomotion and that this function may be shared across pathways.

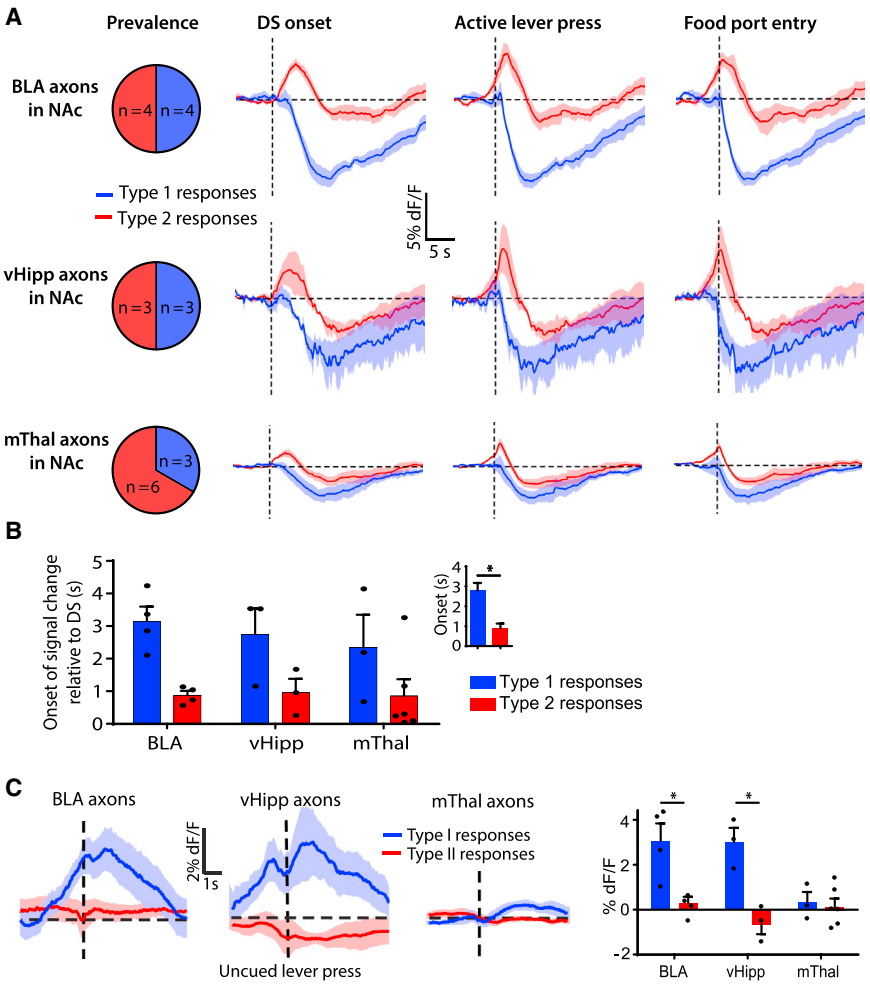

Figure 3. The Heterogeneity of NAc Input Activity Is Comparable across Pathways

(A) Mice were classified as having type 1 or type 2 input activity based on the direction of the mean signal change following DS presentations. The average input activity by pathway and response type aligned with the different components of a rewarded trial. See also Figure S1. Shaded areas represent SEM.

(B) Summary of the timing of signal changes (2 SDs) relative to DS presentations. The inset highlights the significant difference in timing between the type 1 and type 2 response patterns. Error bars represent SEM. *p < 0.05.

(C) A difference in input activity between type 1 and type 2 recordings was evident in BLA and vHipp axons when mice made uncued lever presses. Summary data represent the mean signal over the first 2 s after uncued lever presses. *p < 0.05.

performance stabilized (n = 6 to 9 animals per pathway). During these sessions, mice responded to twice as many DS presentations as NS ones, and almost exclusively on the active lever (Figure 2B; 2-way ANOVA; significant interaction, $F_{(1,22)}$ = 68.87, p < 0.001; Sidak *post hoc* tests show the effect of tone type for active lever presses). The latencies between tone onsets and active lever presses were similar following DS and NS presentations (Figure 2B; paired t test, t_{22} = 1.04, p = 0.31). Reward deliveries were signaled by active lever retraction, and, thus, mice exhibited shorter latencies to check the food port following DS-cued versus NS-cued lever presses (paired t test, t_{22} = 9.01, p < 0.001).

We aligned the movement-corrected axonal calcium signals to instances when the DS or NS was presented, separated based on how the mouse responded: active lever press, inactive lever press, or no response. In every recording, the most pronounced changes in axonal activity occurred around periods of reward consumption, which followed DS presentations and an active lever press (Figure 2C). These changes in input activity were highly consistent from trial to trial and across days (Figure S1A). Between animals, however, there were clear examples of divergent activity around reward delivery within each group of pathway-specific recordings. To characterize this heterogeneity, we classified each mouse as having type 1 or type 2 activity based on whether the first abrupt change in the mean of the signal following rewarded DS presentations was negative or positive, respectively. Data from individual mice were pooled over two to three sessions for all analyses of input activity.

There was a similar proportion of type 1 and type 2 classified recordings across pathways (χ^2_{22} = 0.62, p = 0.73), and the two types of input activity clearly diverged on rewarded trials (Figure 3A). The timing of these signals also differed in relation to DS presentations (Figure 3B; 2-way ANOVA; main effect of response type, $F_{(1,17)}$ = 14.72, p = 0.001, no pathway effect; no interaction effect, $F_{(2,17)}$ = 0.25, p = 0.78), but it was not clear whether the different activity patterns were coupled to different components of the rewarded trial (Figure 3A). Task performance did not relate to recording classification in any way (Figure S1B).

Outside of rewarded trials, changes in GCaMP fluorescence were relatively small. However, increases in activity were evident around uncued lever presses (those made outside of tone presentations) in the type 1 classified BLA and vHipp input recordings (Figure 3C; 2-way ANOVA; significant interaction, $F_{(2,17)}$ = 4.87, p = 0.02; Sidak *post hoc* tests show the effect of response type in BLA and vHipp input). There was no detectable change in any of the inputs following ignored DS presentations (Figure 2C), but NS presentations elicited activity in a majority of BLA and mThal input recordings (mostly type 2), particularly when mice responded with a lever press (Figure S1C). These signal changes outside of reward delivery were at the detection limit of the technique, and the variability among the recordings of each pathway (across mice) made it difficult to identify clear distinctions between pathways. This between-animal variability in pathway-specific activity

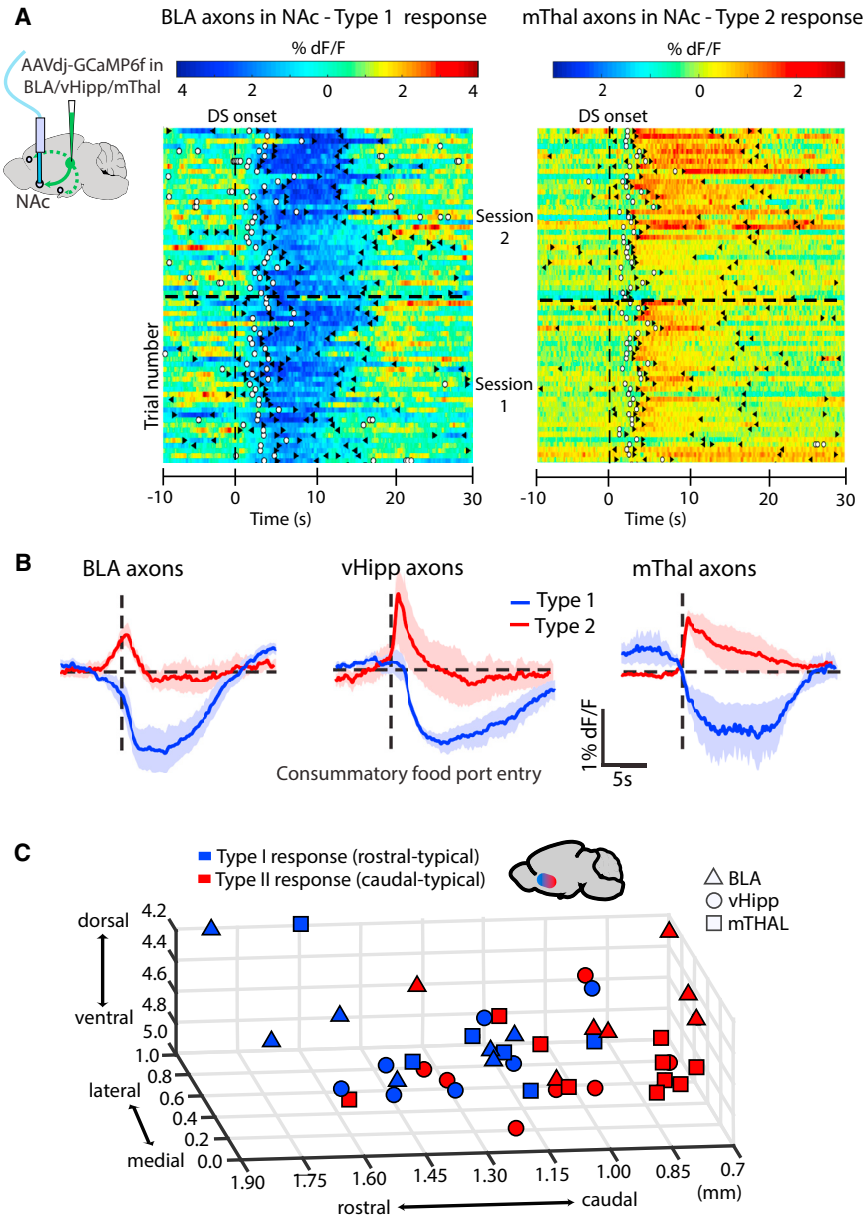

Figure 4. Afferent Activity Is Divergent along the Rostrocaudal Axis of the NAc Shell

(A) Schematic of the additional recordings using AAVdj-hSyn-GCaMP6f (left). Color plots highlight the consistency of input activity in representative mice by showing trial-by-trial changes in GCaMP6f fluorescence across rewarded DS presentations (open circles indicate lever presses; triangles bracket food port visits).

(B) Average pathway-specific GCaMP6f fluorescence aligned to consummatory food port entries according to response pattern. As with the GCaMP6s recordings, these changes in input activity were well-defined and used to classify response type. Shaded areas represent SEM.

(C) Location of each recording probe in the NAc labeled according to pathway and response type for all GCaMP data. Across all recordings, a relationship was evident between rostrocaudal recording location in the NAc and the input activity on rewarded trials.

See also Figure S2.

suggests that mixed or even opposing activity may be a regular feature of these inputs (Ciocchi et al., 2015; Otis et al., 2017). Note that population-level recordings can underestimate event-related neural activity when it consists of axons with opposing activity.

Input Activity Patterns Differ along the Rostrocaudal Axis of the NAc Shell

In light of the abundant literature showing rostrocaudal distinctions in NAc shell-mediated feeding behavior (Castro and Berridge, 2014; Castro et al., 2016; Ho and Berridge, 2014; Peciña and Berridge, 2005; Reynolds and Berridge, 2001, 2002, 2003; Vaccarino, 1994), we explored the possibility that type 1 and type 2 input activity relates to recording location in the NAc. We ran additional cohorts of mice, purposefully varying recording probe location in the NAc shell (n = 6 to 8 animals per pathway). We also used the GCaMP6f variant (Chen et al., 2013) with the hope that its faster kinetics would help us disentangle the contribution of task events that occur close in time.

As with the previous data, the recordings from each animal showed consistent changes in motion-corrected GCaMP6f signal around periods of reward obtainment (Figure 4A). There was again variability between animals, so mice were classified as having type 1 or 2 activity based on the sign of the first significant mean signal change following rewarded DS presentations (Figure 4B).

Recording fiber location in the NAc was assessed in every animal (GCaMP6s and GCaMP6f) and plotted in coordinate space, with labels indicating response type and pathway (Figure 4C; Figure S2). Type 1 and type 2 recordings were associated with more rostral and more caudal NAc shell placements, respectively. A multiple logistic regression was used to formally assess probe location in relation to response type. When data were pooled across pathways, this analysis identified the rostrocaudal axis as being a significant predictor of response category (i.e., there was a significant regression coefficient for the rostrocaudal axis, $B = -11.02$, $p = 0.004$; this factor was not significant for any individual pathway). Overall, the data suggest that, in relation to reward obtainment, excitatory input to the NAc shell may be better characterized by rostrocaudal position in the NAc than by the source of the afferent fibers.

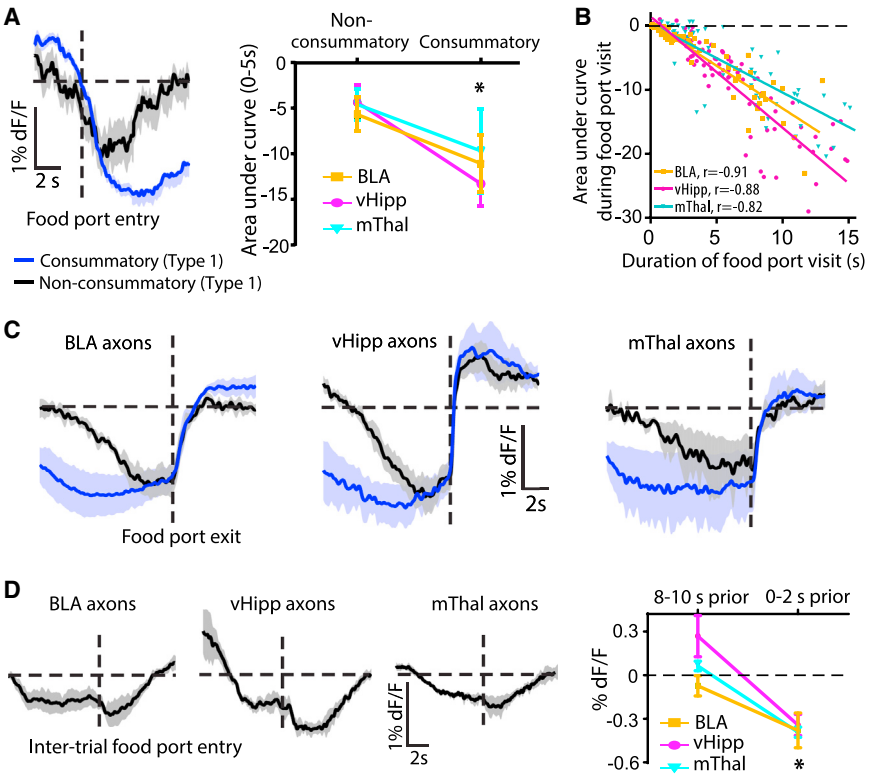

Figure 5. Time-Locked Reductions in Input to the Rostral NAc Shell Occur during Every Food Port Visit

(A) Example of change in BLA input GCaMP6f fluorescence in the rostral NAc shell in relation to food port visits following rewarded and unrewarded lever presses (left). Also shown is a summary of all type 1 changes in input activity associated with these food port visits (right). See also Figures S3 and S4. Shaded areas of line graphs and error bars represent SEM. *$p < 0.05$.

(B) Correlations between the duration of every food port visit and the concomitant change in input activity for a representative type 1 recording session from each pathway. Across all type 1 recordings, b = −1.55 ± 0.32; average r = −0.80.

(C) Average GCaMP6f fluorescence aligned to exits from the food port after consummatory and non-consummatory visits for the type 1 recordings of each pathway.

(D) Average and summary of GCaMP6f fluorescence in relation to uncued, inter-trial food port visits for the type 1 recordings of each pathway, which suggests that reduced excitatory drive in the rostral NAc shell promotes food seeking. The summary data represent signal mean in the indicated period.

Input Activity on Rewarded Trials Primarily Coincides with the Food Port Visit

In rewarded trials, the DS presentation, active lever press, and food port visit typically occurred within a 5-s period (Figures 2B and 2C), which made it hard to identify the unique contribution of each event to the changes in input activity (Figure 3A). To disentangle the contribution of each type of event, we used statistical regressions to create generalized linear models of the GCaMP fluorescence for the rewarded trials of each recording (Parker et al., 2016). This statistical disambiguation takes advantage of trial-to-trial variability in the behavior (i.e., latency between DS, lever press, and food port visit) to identify the characteristic signal change associated with each type of task event.

On average, the statistical modeling attributed most of the signal variance across rewarded trials to food port entrances and exits (Figure S3A). Although there were instances where clear changes in input activity were attributed to the DS onset and lever press, particularly in the GCaMP6s recordings, this activity was not consistent across the different recordings of each input (Figure S3B). These findings are in line with previous research showing that the most widespread and coherent changes in NAc neuron activity tend to coincide with feeding (London et al., 2018; Nicola et al., 2004a, 2004b).

Reductions in Excitatory Input in the Rostral NAc Shell Persist throughout Food Port Visits

To determine whether the food port-associated input activity was contingent on the presence of food, we aligned input activity to different types of food port visits. In the type 1 rostral-typical recordings, food port-associated reductions in excitatory input were more pronounced during consummatory visits than the non-consummatory ones that followed unrewarded lever presses (Figure 5A; 2-way ANOVA; main effect of consumption, $F_{(1,7)} = 11.13$, $p = 0.013$, but not pathway; no interaction effect, $F_{(2,7)} = 0.44$, $p = 0.66$). However, input activity during food port visits in type 1 recordings was highly correlated with visit length, irrespective of whether a reward was consumed (Figure 5B; mean slope, b, of best fit lines = −1.55 ± 0.32; average r = −0.80, calculated from *Z* score transformations). In the moments before animals exited the food port, type 1 input activity was indistinguishable between consummatory and non-consummatory food port visits (Figure 5C). Together, these findings are consistent with the idea that a reduction in rostral NAc shell activity promotes both the initiation and maintenance of feeding behavior (Krause et al., 2010; Nicola et al., 2004b; Taha and Fields, 2005). In line with this hypothesis, there were small reductions in input activity in these recordings in the seconds leading up to the food port visits that occurred in between trials, at times that did not closely follow lever press events or tone presentations (Figure 5D; 2-way ANOVA; main effect of time, $F_{(1,7)} = 37.25$, $p < 0.001$, but not pathway; no interaction effect, $F_{(2,7)} = 1.38$, $p = 0.31$).

In the type 2 caudal typical recordings, food port-associated input activity was not different between consummatory and non-consummatory food port visits (Figure S4A). Unlike the input activity of type 1 recordings, these signal changes did not persist during periods of consumption (Figure S4B) and did not correlate with food port visit duration (b = 0.13 ± 0.33, average r = 0.03).

Suppressing Pathway-Specific Excitatory Input to the NAc Shell Increases Food Intake

Given the dynamic changes in input activity during food port visits, we decided to test whether pathway-specific disruptions of input activity influence free feeding behavior. Specifically, do reductions in rostral NAc shell input promote feeding, and do reductions in caudal NAc shell input suppress it?

We drove expression of the inhibitory opsin eArchT3.0 in the BLA, vHipp, or mThal in different cohorts of mice so that light delivered to the NAc would suppress input activity in a pathway-specific manner. Although there is concern that this approach is not particularly effective and can cause unintended effects (Mahn et al., 2016), we found that yellow light caused an immediate reduction in the amplitude of electrically evoked excitatory postsynaptic currents (eEPSCs) in NAc neuron brain slice recordings from these mice that persisted during, but not beyond, 10 min of constant light delivery (Figures 6A and 6B; 2-way ANOVA; main effect of light, $F_{(2,28)} = 10.92$, $p < 0.001$, but not pathway; no interaction effect, $F_{(4,28)} = 0.39$, $p = 0.81$). There was also a concomitant increase in paired pulse ratio measurements during light delivery, consistent with a presynaptic reduction in vesicle release probability (Figures 6A and 6B; 2-way ANOVA; main effect of light, $F_{(2,28)} = 7.62$, $p = 0.002$, but not pathway; no interaction effect, $F_{(4,28)} = 1.28$, $p = 0.30$). Although it is possible that the activity of this opsin, an outward proton pump, can alter the interstitial environment and generate unintended changes in NAc activity, there was no noticeable change in the physiology of the recorded neurons. Neither acute nor prolonged opsin activation altered the membrane resistance of the recorded neurons or the current needed to maintain them at a stable membrane potential (Figures S5A and S5B).

Mice with this afferent-specific opsin expression and rostral or caudal NAc optic fiber implants were given unlimited access to a sweetened chocolate drink during daily visits to an activity box (Figure 6C). After these animals habituated to the optical tether, we delivered light intracranially in 10-min epochs while monitoring licking behavior (Figure 6D). The mice with rostral NAc shell fiber optic implants drank significantly more during the photo-inhibition epochs than during the intervening periods, irrespective of which pathway was targeted (Figure 6E; 2-way ANOVA; significant interaction, $F_{(3,23)} = 5.43$, $p = 0.006$; Sidak *post hoc* tests show a significant effect of light in each pathway except for the enhanced yellow fluorescent protein [eYFP] control). This increase in consumption paralleled an increase in the number of lick bouts (Figure S5C), indicating that these effects were not driven by an inability to disengage from the feeder. These consumption effects were not present in eYFP control mice, and they were less pronounced in the experimental mice when they had free access to food in their home cage (Figure S5D).

Mice with caudal NAc shell fiber optic implants, in contrast to our expectations, did not consume less during photo-inhibition epochs than the intervening periods (Figure 6E). In fact, there was a slight increase in consumption in these mice overall, but no individual pathway was significant in Sidak *post hoc* tests (2-way ANOVA; significant interaction, $F_{(3,22)} = 3.47$, $p = 0.034$, and main effect of light, $F_{(1,22)} = 8.17$, $p = 0.009$). Overall, the data suggest that reduced input from any excitatory afferent to the NAc shell is sufficient to promote food consumption, with the rostral NAc shell being particularly sensitive to this effect.

Network Activity Is Coordinated Upstream of the NAc during Food Port Visits

Because food port-associated input activity is variable across the NAc but similar between pathways, it is possible that input activity is coordinated by local signaling molecules acting presynaptically. Many signaling molecules in the NAc can regulate presynaptic calcium dynamics, including dopamine, acetylcholine, gamma-aminobutyric acid (GABA), opioids, and endocannabinoids (Britt and McGehee, 2008; Catterall and Few, 2008; Quiroz et al., 2016). Another possibility is that input activity is coordinated upstream of the NAc in distinct populations of rostral and caudal NAc-projecting neurons throughout the forebrain.

To explore this issue, we first assessed whether inputs to the rostral and caudal NAc shell come from distinct cell populations by injecting different retrograde fluorescent tracers into these areas of the NAc (Figure 7A). Histological analyses of the amygdala, hippocampus, and thalamus revealed that the vast majority of retrogradely labeled cells incorporated only one of the two retrograde tracers (Figure 7B; n = 3 for each injection site), indicating that distinct populations of neurons innervate the rostral and caudal NAc shell. These two populations of neurons were not anatomically segregated in any clear way either within or across coronal brain slices of each region.

To determine whether feeding related network activity is coordinated in the distinct populations of rostral and caudal NAc-projecting neurons throughout the forebrain, we drove GCaMP6f expression in a retrograde manner (Tervo et al., 2016), targeting a virus to the rostral or caudal NAc shell in different cohorts of mice (Figures 8A and 8B). We were unable to obtain sufficient GCaMP expression in thalamic neurons with this approach, but there was expression in the medial prefrontal cortex (mPFC), and we were able to resolve small changes in fluorescence from this region as well as from the BLA and vHipp (n = 6–7 each pathway). Prior to training on the DS-cued operant task, we first recorded projection neuron activity as animals habituated to the operant chamber and received periodic reward deliveries to see whether consumption-related activity is task-dependent. Even during these free feeding sessions, consumption coincided with changes in the activity of NAc-projecting neurons that mimicked the corresponding axonal activity recorded in the NAc (Figure 8C). Consummatory food port visits coincided with reduced activity in all recordings of rostral NAc-projecting neurons and increased activity in all recordings of caudal NAc-projecting neurons (Figure 8D; 2-way ANOVA; main effect of innervation target, $F_{(1,13)} = 15.03$, $p = 0.002$, but not pathway; no interaction, $F_{(2,13)} = 1.91$, $p = 0.188$). These changes in input activity remained evident after animals learned the DS-cued operant task, and they continued to be consistent with the axonal measurements (Figure S6). Together, these findings indicate that feeding-related changes in NAc neuron activity arise from coordinated changes in upstream neurons throughout the forebrain.

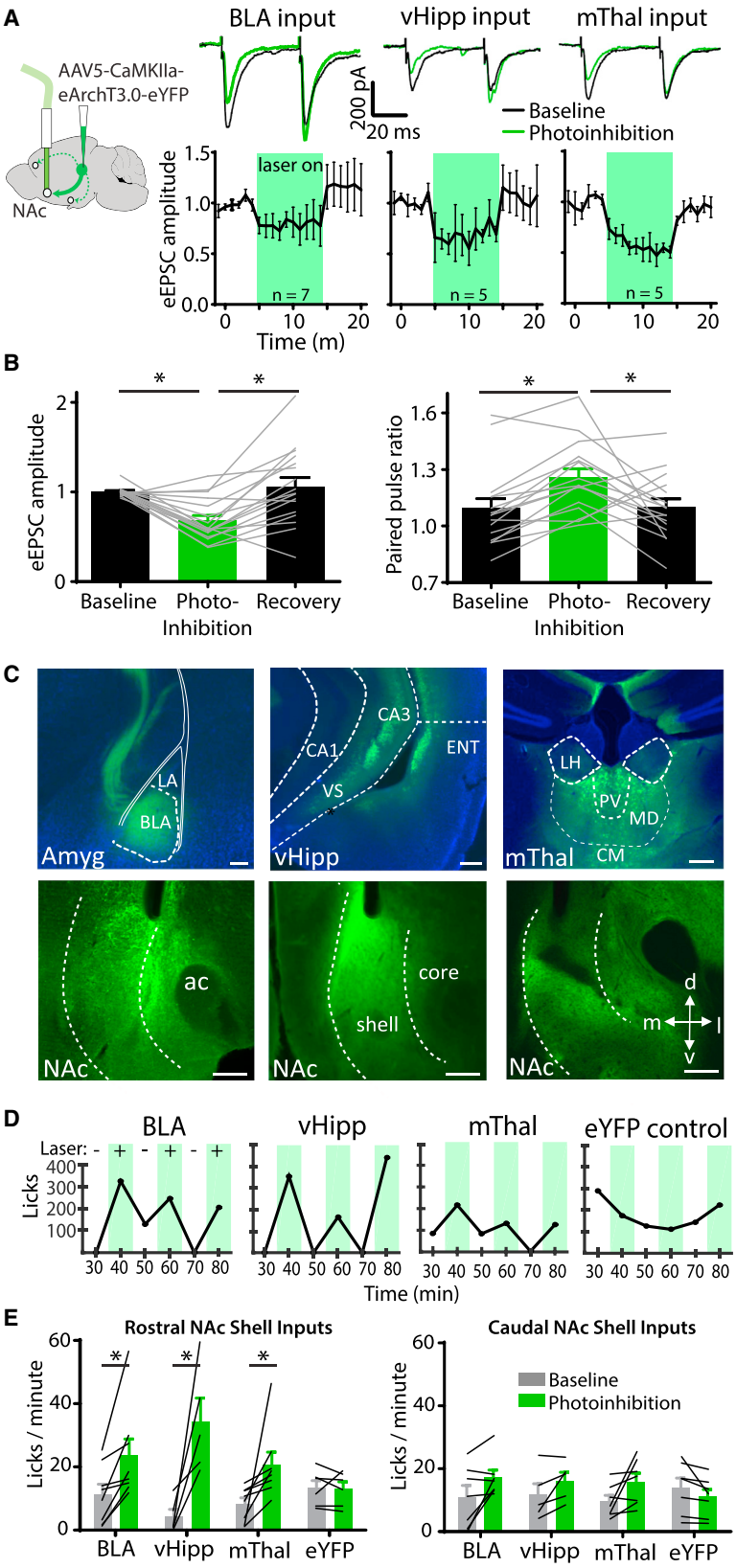

Figure 6. Reducing Pathway-Specific Excitatory Input to the NAc Shell Increases Food Consumption

(A) Schematic of optical fiber placement in the NAc shell of a mouse infected with AAV5-CaMKIIa-eArchT3.0-eYFP in the BLA, vHipp, or mThal (left). Also shown are example traces of paired pulse electrically evoked EPSCs obtained from NAc neuron brain slices from these mice in the absence and presence of yellow light (top) And a summary of all NAc neuron brain slice recording data for each of the examined inputs (bottom). Error bars represent SEM.

(B) Average change in eEPSC amplitudes and paired pulse ratio measurements (P_2/P_1) induced by pathway-specific activation of eArchT3.0 across all brain slice recordings. See also Figure S5. *$p < 0.05$.

(C) Coronal brain slices from representative mice showing eArchT3.0-EYFP fluorescence at the injection site and optic probe placement in the NAc. Scale bars, 200 μm.

(D) Example changes in consummatory behavior caused by photo-inhibition of rostral NAc inputs in alternating 10-min epochs.

(E) Summary of consummatory behavior during baseline and photo-inhibition epochs according to the pathway targeted and the rostral versus caudal placement of the optical fiber in the NAc. *$p < 0.05$.

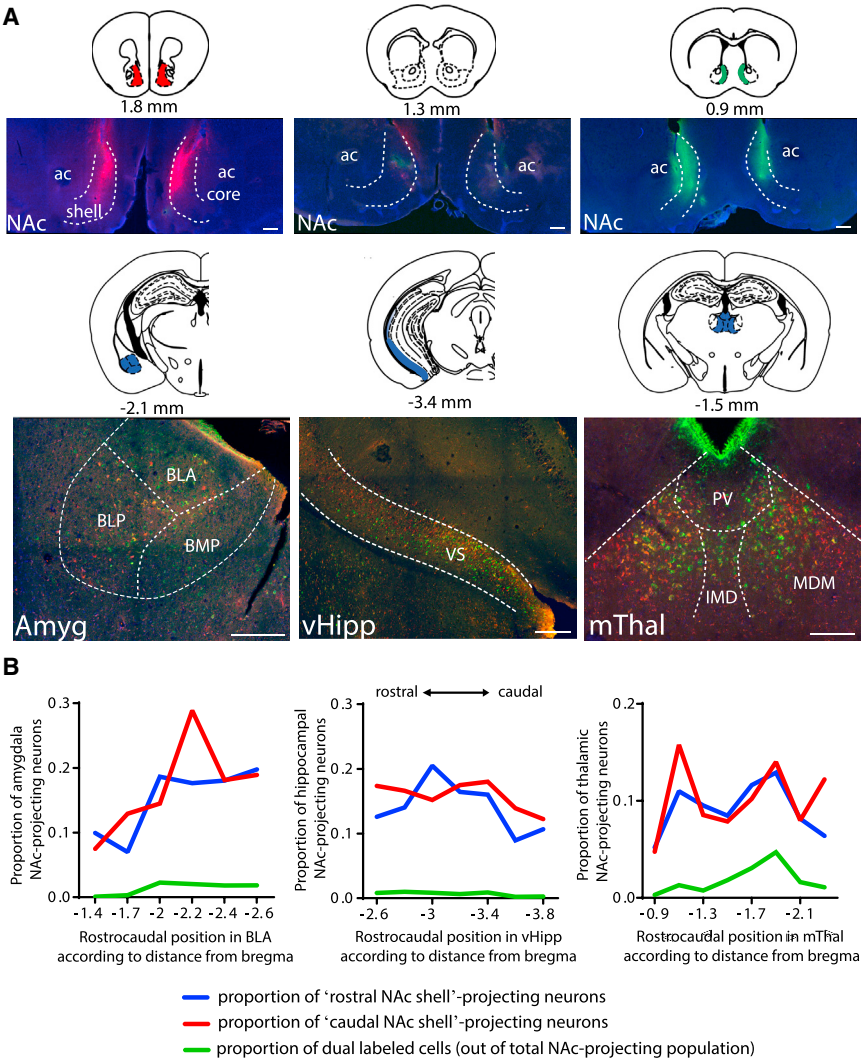

Figure 7. The Rostral and Caudal NAc Shells Are Innervated by Distinct Forebrain Cell Populations

(A) Representative coronal brain slices showing the non-overlapping placement of distinct fluorescent retrograde tracers in the rostral (red, CTB-594nm) and caudal (green, CTB-488nm) NAc shell (top). Distinct populations of retrogradely labeled cells were clustered together in the BLA, vHipp, and mThal (bottom).

(B) The proportion of rostral and caudal NAc-projecting neurons identified across serial sections of each afferent region relative to the total population labeled in each region with each tracer. Labeled cells were intermingled together, but few cells contained both tracers, suggesting that distinct cell populations target the rostral and caudal NAc shell.

DISCUSSION

The NAc regulates reward-seeking behavior and food consumption across a variety of behavioral paradigms. Spiking activity in the NAc is driven by a diverse collection of excitatory inputs that have been implicated in a range of psychiatric disorders, including depression (Bagot et al., 2015; McDevitt et al., 2014), drug addiction (Pascoli et al., 2011, 2014), eating disorders (Avena and Bocarsly, 2012), and schizophrenia (Chambers et al., 2001; Floresco et al., 2009). To gain insight into what information these inputs encode, we compared fiber photometry recordings and optogenetic manipulations of these pathways during reward-seeking behavior.

Because each input to the NAc is associated with distinct cognitive processes (Floresco, 2015; Humphries and Prescott, 2010), we hypothesized that they would be differentially active at a population level during certain task events. However, pathway-specific input activity is clearly not uniform throughout the NAc. At times there is variable, even opposing input activity within each afferent pathway, in part because distinct populations of neurons throughout the forebrain innervate the rostral and caudal NAc shell. We observed pronounced, consistent changes in input activity during food port visits, and this activity was more variable along the rostrocaudal axis of the NAc than between pathways. Consistent with the known involvement of the NAc in feeding decisions, we show that a reduction in glutamate release from individual pathways is sufficient to increase food consumption, particularly when the rostral NAc shell is affected.

Photometry Recordings of NAc Inputs

We recorded NAc input activity in animals performing a discriminative cue operant reward-seeking task and analyzed pathway-specific changes in relation to tone presentations (DS and NS), lever presses, and food port visits, with distinctions made in each category according to the animals' behavior either before or after each event (Nicola et al., 2004a, 2004b). The most pronounced and consistent changes in input activity in all pathways coincided with food port visits, particularly the consummatory ones that followed DS-cued active lever presses. This input activity was divergent along the rostrocaudal axis of the NAc but largely similar between pathways. Food port visits, even non-consummatory ones, were time-locked to reductions in excitatory input in the rostral NAc shell. In the caudal NAc shell, there were transient increases in excitatory input whenever mice entered the food port, but these did not persist for the duration of the visit. The similarities in input activity between pathways may reflect the abundant interconnectivity between the forebrain regions that innervate the NAc (Beyeler et al., 2016; Ciocchi et al., 2015; Do-Monte et al., 2017; Kirouac, 2015; Li and Kirouac, 2012; Otis et al., 2017).

One goal of this work was to determine whether there is distinctive activity in the different pathways at a population level

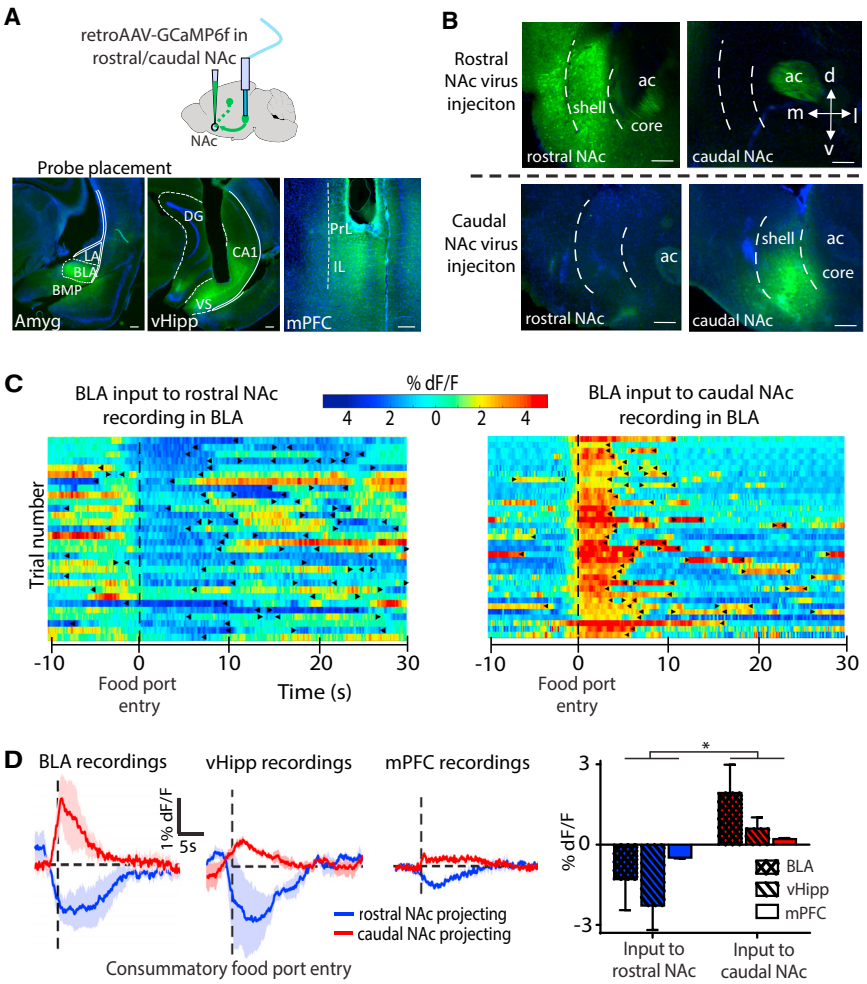

Figure 8. Coordinated Consumption-Related Changes in Afferent Input to the Rostral and Caudal NAc Shell Are Evident in Upstream Regions

(A) Schematic of a mouse infected with retroAAV-hSyn1-GCaMP6f in the rostral or caudal NAc shell and optic probe placement in an upstream region (top). Representative coronal brain slices show GCaMP6f fluorescence in the regions upstream of the NAc where the optic probe was placed (bottom). DG, dentate gyrus; PrL, prelimbic; IL, infralimbic. Scale bars, 200 μm.

(B) Coronal brain slices showing localization of GCaMP fluorescence at the injection site in either the rostral or caudal NAc. Scale bars, 200 μm.

(C) Color plots show example changes in GCaMP6f fluorescence in the amygdala aligned to consummatory food port entries during a training session specifically from neurons that innervate the rostral (left) or caudal (right) NAc shell. The dashed vertical line at the zero time point and rightward-pointing triangles signify food port entrances. Leftward-pointing triangles signify food port exits.

(D) Average and summary of GCaMP6f fluorescence in relation to consummatory food port visits recorded in forebrain regions upstream of the NAc from neurons that specifically innervate the rostral or caudal NAc shell. Summary data represent the mean signal over the first 5 s after food port entry. Shaded areas of line graphs and error bars represent SEM. *$p < 0.05$.

See also Figure S6.

relative to task events, which could provide insight into the information encoded in each input. However, we found that the variability between pathways was less pronounced than the variability within each pathway across different areas of the NAc. These data suggest that the heterogeneity in spiking activity typically found among NAc neurons during reward seeking may arise from divergent input activity within each afferent pathway (Guillem et al., 2014; Morrison et al., 2017; Nicola et al., 2004a, 2004b; West and Carelli, 2016). Likewise, the heterogeneity observed among neurons in upstream forebrain areas may be representative of the NAc input activity from these regions (Ambroggi et al., 2008; Ciocchi et al., 2015; Do-Monte et al., 2017; Kim et al., 2017; Li et al., 2016; Otis et al., 2017; Tye et al., 2010). Our retrograde tracing data are consistent with this idea because they reveal that different NAc subregions are innervated by distinct but intermingled upstream neurons.

There are many reasons why we are confident that the photometry signals captured accurate population changes in intracellular calcium- and pathway-specific activity. First, the 405-nm isosbestic signal (Kim et al., 2016) exhibited relatively minor fluctuations in activity that were often uncorrelated with or opposite to the changes observed in the calcium-sensitive signal. Second, the opposing changes in axonal activity measured in the rostral and caudal ends of the NAc shell complemented the opposing activity observed in the cell body recordings of rostral and caudal NAc-projecting neurons. Furthermore, task-relevant changes in the GCaMP signals were consistent within and between sessions, regardless of the specific recording equipment or types of food receptacles used. Additionally, different viral constructs and GCaMP6 variants produced comparable data.

Electrophysiological recordings in rats performing a similar discriminative stimulus operant task have demonstrated that changes in spiking activity in the NAc are most prevalent and synchronous during food port visits (Nicola et al., 2004a, 2004b). Also, a recent meta-analysis found that, regardless of the behavioral task, the most prevalent response pattern in the NAc during consumption is a reduction in spiking activity (London et al., 2018). Events preceding consumption, such as operant and approach behavior, are typically associated with sparser and more heterogeneous changes in activity (London et al., 2018; Nicola et al., 2004a, 2004b). The fiber photometry approach used here is well suited to characterizing coherent population-level changes in activity, and the most consistent and well-defined activity patterns we observed occurred during food port visits.

It is known that NAc neurons are responsive to unrewarded DS presentations (Nicola et al., 2004a), but this activity was not

noticeable in any of our input-specific recordings even though it has been demonstrated in multiple areas that project to the NAc (Ambroggi et al., 2008; Ishikawa et al., 2008b). One issue is that these changes in activity are relatively brief, involving just a few more or less action potentials in a small proportion of neurons, which may be below the sensitivity of the technique. Because small changes in NAc spiking are known to reflect important differences in reward value and likelihood of approach behavior, it is likely that there are meaningful differences in pathway activity that we could not resolve (Ambroggi et al., 2008; Ishikawa et al., 2008a; Nicola et al., 2004a).

NAc Involvement in Feeding Behavior

The similarity we observed in food port-associated input activity between pathways was just as striking as the divergence in input activity between the rostral and caudal ends of the NAc shell. Distinct roles for these areas of the NAc have been suggested by inactivation studies, with the rostral pole being particularly important for feeding behavior (Faure et al., 2010; Reynolds and Berridge, 2001, 2003).

The amount of food animals will eat is strongly influenced by neural activity in the rostral NAc shell (Maldonado-Irizarry et al., 1995; O'Connor et al., 2015; Reynolds and Berridge, 2001; Stratford and Kelley, 1999; Stratford et al., 1998). Both optical and pharmacological manipulations that reduce activity in the rostral NAc shell potently increase food intake, even in food-sated rodents (Kelley and Swanson, 1997; O'Connor et al., 2015; Reynolds and Berridge, 2001, 2003; Stratford et al., 1998). Conversely, electrical and optical manipulations that increase activity in this area instantaneously terminate ongoing bouts of feeding and dramatically reduce overall food intake, even in food-deprived rodents (Krause et al., 2010; O'Connor et al., 2015). Feeding is likely regulated by these neurons because they are a source of inhibitory drive onto downstream, possibly orexigenic, hypothalamus neurons (Castro et al., 2015; Zheng et al., 2007). Much less is known about how inputs to the NAc influence consummatory behavior, although there is increasing interest in this topic (Do-Monte et al., 2017; Labouèbe et al., 2016; Parker et al., 2015; Tellez et al., 2016).

It has been hypothesized that the reductions in NAc neuron activity necessary for feeding result from peptidergic (Urstadt and Stanley, 2015) and GABAergic signaling (Faure et al., 2010), either through feedforward inhibition (Dobbs et al., 2016) or long-range projections (Churchill and Kalivas, 1994; Morales and Margolis, 2017; van Zessen et al., 2012). However, our data suggest that the reduction in rostral NAc activity necessary for feeding arises in part from a marked reduction in glutamate input from multiple sources. This reduction in NAc input during feeding is orchestrated upstream of the NAc because it is evident in neurons that innervate the rostral NAc shell throughout the forebrain. These data are consistent with reports that increased activity in brain regions upstream of the NAc reduce food intake (Sweeney and Yang, 2015; White and Fisher, 1969).

We also found that pathway-specific, optogenetic reductions of glutamate release could increase food intake, irrespective of the pathway targeted. The similarity of the effect between pathways raises the concern that axonal eArchT3.0 activation may produce unintended, non-specific changes in NAc physiology. As an outward proton pump, this opsin has been shown to significantly alkalize the intracellular space, which may increase the rate of spontaneous vesicle release while reducing evoked release (Mahn et al., 2016). Another concern is that the opsin might acidify the extracellular environment. Acid-sensing ion channels are expressed in the NAc and are known to contribute to EPSCs (Kreple et al., 2014); however they fully desensitize within seconds (Gründer and Chen, 2010). In brain slice recordings, we did not find any overt change in NAc neuron physiology during input-specific opsin activation. Behaviorally, the reductions in input activity increased food intake relative to intervening periods. These effects were less pronounced in food-sated mice and small in relation to the effects reported following infusion of GABA receptor agonists or glutamate receptor antagonists into the rostral NAc shell (Kelley and Swanson, 1997; Reynolds and Berridge, 2001, 2003; Stratford et al., 1998). These data suggest that the initiation and maintenance of food consumption are sensitive to the sum of the glutamate signaling in the rostral NAc shell. It is possible that consensus activity among the interconnected forebrain regions that innervate this region may be a requirement for feeding behavior.

The data presented here underscore the coordinated nature of excitatory input to the NAc during particular facets of reward-seeking behavior. The operant task used clearly recruits and depends on multiple excitatory inputs to the NAc (Ambroggi et al., 2008; Ishikawa et al., 2008a, 2008b), which makes it difficult to determine what specific information is encoded in each excitatory input. It will be useful to identify tasks that uniquely activate particular inputs to the NAc. Although it is necessary to counteract or mimic pathway-specific changes in activity to confirm function, it is important to recognize that certain behaviors, such as food seeking, may be sensitive to changes in glutamate input from any pathway. There is also now considerable evidence that discrete pathways are often comprised of fibers that convey opposing information (Do-Monte et al., 2017; Labouèbe et al., 2016), which underscores the importance of tracking single-cell activity or targeting recordings and manipulations to fibers defined by specific activity patterns.

STAR★METHODS

Detailed methods are provided in the online version of this paper and include the following:

- KEY RESOURCES TABLE
- CONTACT FOR REAGENT AND RESOURCE SHARING
- EXPERIMENTAL MODEL AND SUBJECT DETAILS
- METHOD DETAILS
  - Viral Constructs and Surgery
  - Behavioral Testing
  - GCaMP Photometry Recordings
  - Brain Slice Electrophysiology
  - Retrograde Tracing
  - Histology
- QUANTIFICATION AND STATISTICAL ANALYSIS

SUPPLEMENTAL INFORMATION

Supplemental Information includes six figures and can be found with this article online at https://doi.org/10.1016/j.neuron.2018.07.051.

ACKNOWLEDGMENTS

We thank Han-Byul Moon, Jane Su, Saran London, Sasha Burwell, Sandy Wong, Chloe Lau, and Daria Sandra for assistance with the behavioral experiments. We also thank Charu Ramakrishnan for generously providing the AAVDJ-hSyn-GCaMP6f virus. The confocal images for this manuscript were collected in the McGill University Life Sciences Complex Advanced BioImaging Facility (ABIF). This research was supported by the Natural Sciences and Engineering Research Council (RGPIN-05069-2014 to J.P.B. and PGS D3-444759-2013 to S.J.R.), the Fonds de recherche du Québec - Nature et technologies (2017-NC-197714 to J.P.B.), the Canadian Institutes of Health Research (PJT-153241 to J.P.B.), and the Canadian Foundation for Innovation (32477 to J.P.B.).

AUTHOR CONTRIBUTIONS

Conceptualization and Writing, S.J.R. and J.P.B.; Methodology and Software, S.J.R., J.P.B., T.J.D., L.G., and K.D.; Investigation and Analysis, S.J.R., C.K.L., J.A.M., and A.K.Y.; Resources, J.P.B., T.J.D., L.G., and K.D.; Funding Acquisition and Supervision, J.P.B.

DECLARATION OF INTERESTS

The authors declare no competing interests.

Received: October 15, 2017
Revised: June 14, 2018
Accepted: July 27, 2018
Published: August 23, 2018

REFERENCES

Ambroggi, F., Ishikawa, A., Fields, H.L., and Nicola, S.M. (2008). Basolateral amygdala neurons facilitate reward-seeking behavior by exciting nucleus accumbens neurons. Neuron *59*, 648–661.

Ambroggi, F., Ghazizadeh, A., Nicola, S.M., and Fields, H.L. (2011). Roles of nucleus accumbens core and shell in incentive-cue responding and behavioral inhibition. J. Neurosci. *31*, 6820–6830.

Avena, N.M., and Bocarsly, M.E. (2012). Dysregulation of brain reward systems in eating disorders: neurochemical information from animal models of binge eating, bulimia nervosa, and anorexia nervosa. Neuropharmacology *63*, 87–96.

Bagot, R.C., Parise, E.M., Peña, C.J., Zhang, H.X., Maze, I., Chaudhury, D., Persaud, B., Cachope, R., Bolaños-Guzmán, C.A., Cheer, J.F., et al. (2015). Ventral hippocampal afferents to the nucleus accumbens regulate susceptibility to depression. Nat. Commun. *6*, 7062.

Beyeler, A., Namburi, P., Glober, G.F., Simonnet, C., Calhoon, G.G., Conyers, G.F., Luck, R., Wildes, C.P., and Tye, K.M. (2016). Divergent routing of positive and negative information from the amygdala during memory retrieval. Neuron *90*, 348–361.

Britt, J.P., and Bonci, A. (2013). Optogenetic interrogations of the neural circuits underlying addiction. Curr. Opin. Neurobiol. *23*, 539–545.

Britt, J.P., and McGehee, D.S. (2008). Presynaptic opioid and nicotinic receptor modulation of dopamine overflow in the nucleus accumbens. J. Neurosci. *28*, 1672–1681.

Britt, J.P., Benaliouad, F., McDevitt, R.A., Stuber, G.D., Wise, R.A., and Bonci, A. (2012). Synaptic and behavioral profile of multiple glutamatergic inputs to the nucleus accumbens. Neuron *76*, 790–803.

Cacciapaglia, F., Wightman, R.M., and Carelli, R.M. (2011). Rapid dopamine signaling differentially modulates distinct microcircuits within the nucleus accumbens during sucrose-directed behavior. J. Neurosci. *31*, 13860–13869.

Castro, D.C., and Berridge, K.C. (2014). Opioid hedonic hotspot in nucleus accumbens shell: mu, delta, and kappa maps for enhancement of sweetness "liking" and "wanting". J. Neurosci. *34*, 4239–4250.

Castro, D.C., Cole, S.L., and Berridge, K.C. (2015). Lateral hypothalamus, nucleus accumbens, and ventral pallidum roles in eating and hunger: interactions between homeostatic and reward circuitry. Front. Syst. Neurosci. *9*, 90.

Castro, D.C., Terry, R.A., and Berridge, K.C. (2016). Orexin in rostral hotspot of nucleus accumbens enhances sucrose 'liking' and intake but scopolamine in caudal shell shifts 'liking' toward 'disgust' and 'fear'. Neuropsychopharmacology *41*, 2101–2111.

Catterall, W.A., and Few, A.P. (2008). Calcium channel regulation and presynaptic plasticity. Neuron *59*, 882–901.

Chambers, R.A., Krystal, J.H., and Self, D.W. (2001). A neurobiological basis for substance abuse comorbidity in schizophrenia. Biol. Psychiatry *50*, 71–83.

Chen, T.W., Wardill, T.J., Sun, Y., Pulver, S.R., Renninger, S.L., Baohan, A., Schreiter, E.R., Kerr, R.A., Orger, M.B., Jayaraman, V., et al. (2013). Ultrasensitive fluorescent proteins for imaging neuronal activity. Nature *499*, 295–300.

Chuhma, N., Tanaka, K.F., Hen, R., and Rayport, S. (2011). Functional connectome of the striatal medium spiny neuron. J. Neurosci. *31*, 1183–1192.

Churchill, L., and Kalivas, P.W. (1994). A topographically organized gamma-aminobutyric acid projection from the ventral pallidum to the nucleus accumbens in the rat. J. Comp. Neurol. *345*, 579–595.

Ciocchi, S., Passecker, J., Malagon-Vina, H., Mikus, N., and Klausberger, T. (2015). Brain computation. Selective information routing by ventral hippocampal CA1 projection neurons. Science *348*, 560–563.

Do-Monte, F.H., Minier-Toribio, A., Quiñones-Laracuente, K., Medina-Colón, E.M., and Quirk, G.J. (2017). Thalamic regulation of sucrose seeking during unexpected reward omission. Neuron *94*, 388–400.e4.

Dobbs, L.K., Kaplan, A.R., Lemos, J.C., Matsui, A., Rubinstein, M., and Alvarez, V.A. (2016). Dopamine regulation of lateral inhibition between striatal neurons gates the stimulant actions of cocaine. Neuron *90*, 1100–1113.

Drai, D., Benjamini, Y., and Golani, I. (2000). Statistical discrimination of natural modes of motion in rat exploratory behavior. J. Neurosci. Methods *96*, 119–131.

du Hoffmann, J., and Nicola, S.M. (2014). Dopamine invigorates reward seeking by promoting cue-evoked excitation in the nucleus accumbens. J. Neurosci. *34*, 14349–14364.

Faure, A., Richard, J.M., and Berridge, K.C. (2010). Desire and dread from the nucleus accumbens: cortical glutamate and subcortical GABA differentially generate motivation and hedonic impact in the rat. PLoS ONE *5*, e11223.

Floresco, S.B. (2015). The nucleus accumbens: an interface between cognition, emotion, and action. Annu. Rev. Psychol. *66*, 25–52.

Floresco, S.B., Zhang, Y., and Enomoto, T. (2009). Neural circuits subserving behavioral flexibility and their relevance to schizophrenia. Behav. Brain Res. *204*, 396–409.

Francis, T.C., and Lobo, M.K. (2017). Emerging role for nucleus accumbens medium spiny neuron subtypes in depression. Biol. Psychiatry *81*, 645–653.

Gründer, S., and Chen, X. (2010). Structure, function, and pharmacology of acid-sensing ion channels (ASICs): focus on ASIC1a. Int. J. Physiol. Pathophysiol. Pharmacol. *2*, 73–94.

Guillem, K., Ahmed, S.H., and Peoples, L.L. (2014). Escalation of cocaine intake and incubation of cocaine seeking are correlated with dissociable neuronal processes in different accumbens subregions. Biol. Psychiatry *76*, 31–39.

Haight, J.L., Fuller, Z.L., Fraser, K.M., and Flagel, S.B. (2017). A food-predictive cue attributed with incentive salience engages subcortical afferents and efferents of the paraventricular nucleus of the thalamus. Neuroscience *340*, 135–152.

Ho, C.Y., and Berridge, K.C. (2014). Excessive disgust caused by brain lesions or temporary inactivations: mapping hotspots of the nucleus accumbens and ventral pallidum. Eur. J. Neurosci. *40*, 3556–3572.

Humphries, M.D., and Prescott, T.J. (2010). The ventral basal ganglia, a selection mechanism at the crossroads of space, strategy, and reward. Prog. Neurobiol. *90*, 385–417.

Ishikawa, A., Ambroggi, F., Nicola, S.M., and Fields, H.L. (2008a). Contributions of the amygdala and medial prefrontal cortex to incentive cue responding. Neuroscience *155*, 573–584.

Ishikawa, A., Ambroggi, F., Nicola, S.M., and Fields, H.L. (2008b). Dorsomedial prefrontal cortex contribution to behavioral and nucleus accumbens neuronal responses to incentive cues. J. Neurosci. *28*, 5088–5098.

Jones, J.L., Day, J.J., Wheeler, R.A., and Carelli, R.M. (2010). The basolateral amygdala differentially regulates conditioned neural responses within the nucleus accumbens core and shell. Neuroscience *169*, 1186–1198.

Kelley, A.E., and Swanson, C.J. (1997). Feeding induced by blockade of AMPA and kainate receptors within the ventral striatum: a microinfusion mapping study. Behav. Brain Res. *89*, 107–113.

Kim, C.K., Yang, S.J., Pichamoorthy, N., Young, N.P., Kauvar, I., Jennings, J.H., Lerner, T.N., Berndt, A., Lee, S.Y., Ramakrishnan, C., et al. (2016). Simultaneous fast measurement of circuit dynamics at multiple sites across the mammalian brain. Nat. Methods *13*, 325–328.

Kim, C.K., Ye, L., Jennings, J.H., Pichamoorthy, N., Tang, D.D., Yoo, A.W., Ramakrishnan, C., and Deisseroth, K. (2017). Molecular and circuit-dynamical identification of top-down neural mechanisms for restraint of reward seeking. Cell *170*, 1013–1027.e14.

Kirouac, G.J. (2015). Placing the paraventricular nucleus of the thalamus within the brain circuits that control behavior. Neurosci. Biobehav. Rev. *56*, 315–329.

Krause, M., German, P.W., Taha, S.A., and Fields, H.L. (2010). A pause in nucleus accumbens neuron firing is required to initiate and maintain feeding. J. Neurosci. *30*, 4746–4756.

Kreple, C.J., Lu, Y., Taugher, R.J., Schwager-Gutman, A.L., Du, J., Stump, M., Wang, Y., Ghobbeh, A., Fan, R., Cosme, C.V., et al. (2014). Acid-sensing ion channels contribute to synaptic transmission and inhibit cocaine-evoked plasticity. Nat. Neurosci. *17*, 1083–1091.

Labouèbe, G., Boutrel, B., Tarussio, D., and Thorens, B. (2016). Glucose-responsive neurons of the paraventricular thalamus control sucrose-seeking behavior. Nat. Neurosci. *19*, 999–1002.

Li, S., and Kirouac, G.J. (2012). Sources of inputs to the anterior and posterior aspects of the paraventricular nucleus of the thalamus. Brain Struct. Funct. *217*, 257–273.

Li, Y., Lindemann, C., Goddard, M.J., and Hyland, B.I. (2016). Complex multiplexing of reward-cue- and licking-movement-related activity in single midline thalamus neurons. J. Neurosci. *36*, 3567–3578.

London, T.D., Licholai, J.A., Szczot, I., Ali, M.A., LeBlanc, K.H., Fobbs, W.C., and Kravitz, A.V. (2018). Coordinated ramping of dorsal striatal pathways preceding food approach and consumption. J. Neurosci. *38*, 3547–3558.

Mahn, M., Prigge, M., Ron, S., Levy, R., and Yizhar, O. (2016). Biophysical constraints of optogenetic inhibition at presynaptic terminals. Nat. Neurosci. *19*, 554–556.

Maldonado-Irizarry, C.S., Swanson, C.J., and Kelley, A.E. (1995). Glutamate receptors in the nucleus accumbens shell control feeding behavior via the lateral hypothalamus. J. Neurosci. *15*, 6779–6788.

Mannella, F., Gurney, K., and Baldassarre, G. (2013). The nucleus accumbens as a nexus between values and goals in goal-directed behavior: a review and a new hypothesis. Front. Behav. Neurosci. *7*, 135.

McDevitt, R.A., Reed, S.J., and Britt, J.P. (2014). Optogenetics in preclinical neuroscience and psychiatry research: recent insights and potential applications. Neuropsychiatr. Dis. Treat. *10*, 1369–1379.

McGinty, V.B., Lardeux, S., Taha, S.A., Kim, J.J., and Nicola, S.M. (2013). Invigoration of reward seeking by cue and proximity encoding in the nucleus accumbens. Neuron *78*, 910–922.

Morales, M., and Margolis, E.B. (2017). Ventral tegmental area: cellular heterogeneity, connectivity and behaviour. Nat. Rev. Neurosci. *18*, 73–85.

Morrison, S.E., and Nicola, S.M. (2014). Neurons in the nucleus accumbens promote selection bias for nearer objects. J. Neurosci. *34*, 14147–14162.

Morrison, S.E., McGinty, V.B., du Hoffmann, J., and Nicola, S.M. (2017). Limbic-motor integration by neural excitations and inhibitions in the nucleus accumbens. J. Neurophysiol. *118*, 2549–2567.

Muir, J., Lorsch, Z.S., Ramakrishnan, C., Deisseroth, K., Nestler, E.J., Calipari, E.S., and Bagot, R.C. (2017). In vivo fiber photometry reveals signature of future stress susceptibility in nucleus accumbens. Neuropsychopharmacology *43*, 255–263.

Nicola, S.M. (2007). The nucleus accumbens as part of a basal ganglia action selection circuit. Psychopharmacology (Berl.) *191*, 521–550.

Nicola, S.M. (2016). Reassessing wanting and liking in the study of mesolimbic influence on food intake. Am. J. Physiol. Regul. Integr. Comp. Physiol. *311*, R811–R840.

Nicola, S.M., Yun, I.A., Wakabayashi, K.T., and Fields, H.L. (2004a). Cue-evoked firing of nucleus accumbens neurons encodes motivational significance during a discriminative stimulus task. J. Neurophysiol. *91*, 1840–1865.

Nicola, S.M., Yun, I.A., Wakabayashi, K.T., and Fields, H.L. (2004b). Firing of nucleus accumbens neurons during the consummatory phase of a discriminative stimulus task depends on previous reward predictive cues. J. Neurophysiol. *91*, 1866–1882.

O'Connor, E.C., Kremer, Y., Lefort, S., Harada, M., Pascoli, V., Rohner, C., and Lüscher, C. (2015). Accumbal D1R neurons projecting to lateral hypothalamus authorize feeding. Neuron *88*, 553–564.

Otis, J.M., Namboodiri, V.M., Matan, A.M., Voets, E.S., Mohorn, E.P., Kosyk, O., McHenry, J.A., Robinson, J.E., Resendez, S.L., Rossi, M.A., and Stuber, G.D. (2017). Prefrontal cortex output circuits guide reward seeking through divergent cue encoding. Nature *543*, 103–107.

Parker, K.E., McCabe, M.P., Johns, H.W., Lund, D.K., Odu, F., Sharma, R., Thakkar, M.M., Cornelison, D.D., and Will, M.J. (2015). Neural activation patterns underlying basolateral amygdala influence on intra-accumbens opioid-driven consummatory versus appetitive high-fat feeding behaviors in the rat. Behav. Neurosci. *129*, 812–821.

Parker, N.F., Cameron, C.M., Taliaferro, J.P., Lee, J., Choi, J.Y., Davidson, T.J., Daw, N.D., and Witten, I.B. (2016). Reward and choice encoding in terminals of midbrain dopamine neurons depends on striatal target. Nat. Neurosci. *19*, 845–854.

Pascoli, V., Turiault, M., and Lüscher, C. (2011). Reversal of cocaine-evoked synaptic potentiation resets drug-induced adaptive behaviour. Nature *481*, 71–75.

Pascoli, V., Terrier, J., Espallergues, J., Valjent, E., O'Connor, E.C., and Lüscher, C. (2014). Contrasting forms of cocaine-evoked plasticity control components of relapse. Nature *509*, 459–464.

Peciña, S., and Berridge, K.C. (2005). Hedonic hot spot in nucleus accumbens shell: where do mu-opioids cause increased hedonic impact of sweetness? J. Neurosci. *25*, 11777–11786.

Pennartz, C.M., Groenewegen, H.J., and Lopes da Silva, F.H. (1994). The nucleus accumbens as a complex of functionally distinct neuronal ensembles: an integration of behavioural, electrophysiological and anatomical data. Prog. Neurobiol. *42*, 719–761.

Quiroz, C., Orrú, M., Rea, W., Ciudad-Roberts, A., Yepes, G., Britt, J.P., and Ferré, S. (2016). Local control of extracellular dopamine levels in the medial nucleus accumbens by a glutamatergic projection from the infralimbic cortex. J. Neurosci. *36*, 851–859.

Reynolds, S.M., and Berridge, K.C. (2001). Fear and feeding in the nucleus accumbens shell: rostrocaudal segregation of GABA-elicited defensive behavior versus eating behavior. J. Neurosci. *21*, 3261–3270.

Reynolds, S.M., and Berridge, K.C. (2002). Positive and negative motivation in nucleus accumbens shell: bivalent rostrocaudal gradients for GABA-elicited eating, taste "liking"/"disliking" reactions, place preference/avoidance, and fear. J. Neurosci. *22*, 7308–7320.

Reynolds, S.M., and Berridge, K.C. (2003). Glutamate motivational ensembles in nucleus accumbens: rostrocaudal shell gradients of fear and feeding. Eur. J. Neurosci. *17*, 2187–2200.

Richard, J.M., Castro, D.C., Difeliceantonio, A.G., Robinson, M.J., and Berridge, K.C. (2013). Mapping brain circuits of reward and motivation: in the footsteps of Ann Kelley. Neurosci. Biobehav. Rev. *37* (9 Pt A), 1919–1931.

Salamone, J.D., Correa, M., Farrar, A., and Mingote, S.M. (2007). Effort-related functions of nucleus accumbens dopamine and associated forebrain circuits. Psychopharmacology (Berl.) *191*, 461–482.

Stratford, T.R., and Kelley, A.E. (1999). Evidence of a functional relationship between the nucleus accumbens shell and lateral hypothalamus subserving the control of feeding behavior. J. Neurosci. *19*, 11040–11048.

Stratford, T.R., Swanson, C.J., and Kelley, A. (1998). Specific changes in food intake elicited by blockade or activation of glutamate receptors in the nucleus accumbens shell. Behav. Brain Res. *93*, 43–50.

Sugam, J.A., Saddoris, M.P., and Carelli, R.M. (2014). Nucleus accumbens neurons track behavioral preferences and reward outcomes during risky decision making. Biol. Psychiatry *75*, 807–816.

Sweeney, P., and Yang, Y. (2015). An excitatory ventral hippocampus to lateral septum circuit that suppresses feeding. Nat. Commun. *6*, 10188.

Taha, S.A., and Fields, H.L. (2005). Encoding of palatability and appetitive behaviors by distinct neuronal populations in the nucleus accumbens. J. Neurosci. *25*, 1193–1202.

Taverna, S., van Dongen, Y.C., Groenewegen, H.J., and Pennartz, C.M. (2004). Direct physiological evidence for synaptic connectivity between medium-sized spiny neurons in rat nucleus accumbens in situ. J. Neurophysiol. *91*, 1111–1121.

Tellez, L.A., Han, W., Zhang, X., Ferreira, T.L., Perez, I.O., Shammah-Lagnado, S.J., van den Pol, A.N., and de Araujo, I.E. (2016). Separate circuitries encode the hedonic and nutritional values of sugar. Nat. Neurosci. *19*, 465–470.

Tervo, D.G., Hwang, B.Y., Viswanathan, S., Gaj, T., Lavzin, M., Ritola, K.D., Lindo, S., Michael, S., Kuleshova, E., Ojala, D., et al. (2016). A designer AAV variant permits efficient retrograde access to projection neurons. Neuron *92*, 372–382.

Tye, K.M., Cone, J.J., Schairer, W.W., and Janak, P.H. (2010). Amygdala neural encoding of the absence of reward during extinction. J. Neurosci. *30*, 116–125.

Urstadt, K.R., and Stanley, B.G. (2015). Direct hypothalamic and indirect trans-pallidal, trans-thalamic, or trans-septal control of accumbens signaling and their roles in food intake. Front. Syst. Neurosci. *9*, 8.

Vaccarino, F.J. (1994). Nucleus accumbens dopamine-CCK interactions in psychostimulant reward and related behaviors. Neurosci. Biobehav. Rev. *18*, 207–214.

van Zessen, R., Phillips, J.L., Budygin, E.A., and Stuber, G.D. (2012). Activation of VTA GABA neurons disrupts reward consumption. Neuron *73*, 1184–1194.

Volkow, N.D., and Morales, M. (2015). The brain on drugs: from reward to addiction. Cell *162*, 712–725.

West, E.A., and Carelli, R.M. (2016). Nucleus accumbens core and shell differentially encode reward-associated cues after reinforcer devaluation. J. Neurosci. *36*, 1128–1139.

White, N.M., and Fisher, A.E. (1969). Relationship between amygdala and hypothalamus in control of eating behavior. Physiol. Behav. *4*, 199.

Yun, I.A., Nicola, S.M., and Fields, H.L. (2004a). Contrasting effects of dopamine and glutamate receptor antagonist injection in the nucleus accumbens suggest a neural mechanism underlying cue-evoked goal-directed behavior. Eur. J. Neurosci. *20*, 249–263.

Yun, I.A., Wakabayashi, K.T., Fields, H.L., and Nicola, S.M. (2004b). The ventral tegmental area is required for the behavioral and nucleus accumbens neuronal firing responses to incentive cues. J. Neurosci. *24*, 2923–2933.

Zheng, H., Patterson, L.M., and Berthoud, H.R. (2007). Orexin signaling in the ventral tegmental area is required for high-fat appetite induced by opioid stimulation of the nucleus accumbens. J. Neurosci. *27*, 11075–11082.

STAR★METHODS

KEY RESOURCES TABLE

REAGENT or RESOURCE	SOURCE	IDENTIFIER
Bacterial and Virus Strains		
AAV9-hSyn-GCaMP6s	UPenn VectorCore	N/A
AAVDJ-hSyn-GCaMP6f	Charu Ramakrishnan, Karl Deisseroth lab	N/A
AAVrg-hSyn1-GCaMP6f-P2A-nls-dTomato	Addgene	plasmid #51085
AAV5-CaMKIIa-eArchT3.0-EYFP	UNC VectorCore	N/A
Chemicals, Peptides, and Recombinant Proteins		
Cholera toxin B subunit CtB-488, CtB-594	Thermo Fisher Scientific	C22841, C22842
Mowiol (mounting solution)	Sigma-Aldrich	81381-250G
DAPI (component of Mowiol mounting solution)	Sigma-Aldrich	D9542-5mg
DABCO (component of Mowiol mounting solution)	Sigma-Aldrich	290734-100ML
Glycerol (component of Mowiol mounting solution)	Sigma-Aldrich	G6279-500ml
Experimental Models: Organisms/Strains		
Wild-type CB57BL/6J Mice	Charles River Laboratories	N/A
Software and Algorithms		
MATLAB script for GCaMP signal demodulation and offline viewing	Tom Davidson	N/A
MATLAB script for GCaMP analysis	Sean Reed	N/A
Med Associates script for operant conditioning	Sean Reed	N/A
Other		
Photometry patch cords	Thorlabs	BFH48-400

CONTACT FOR REAGENT AND RESOURCE SHARING

Further information and requests for resources and reagents should be directed to the Lead Contact, Jonathan Britt (jonathan.britt@mcgill.ca).

EXPERIMENTAL MODEL AND SUBJECT DETAILS

Wild-type CB57BL/6J male mice (25-30 g, 8 weeks old) were obtained from Charles River Laboratories (Senneville, Quebec) and housed individually in a reverse-light cycle room. One week following surgery, at around 3 to 4 months of age, mice were food restricted to 90% of their original body weight. A daily weight and feeding log was maintained throughout the duration of the experiments. All experiments were conducted in accordance with the Canadian Council of Animal Care and the McGill Animal Care Committee.

METHOD DETAILS

Viral Constructs and Surgery

In preparation for surgery, mice were anesthetized with a ketamine (Ventoquinol, 100mg/kg) and xylazine (Bayer, 10mg/kg) cocktail. They were then secured to a stereotaxic frame (Kropf Instruments) and prepared for intracranial virus injections according to standard stereotaxic procedure. 500 nL of virus was injected unilaterally over a 10 min period using a Nanoject II Injector with an oil-filled glass micropipette (Drummond Scientific, 3-000-203-G/X) pulled to a tip diameter of 10 μm.

For the axonal imaging experiments, either AAV9-hSyn-GCaMP6s (from the UPenn vector core) or AAVDJ-hSyn-GCaMP6f (a gift from Charu Ramakrishnan; both at 2.0×10^{13} GC/ml) were delivered into the BLA (distance from bregma, AP −1.8 mm, ML 2.8 mm, DV −5.1 mm), vHipp (AP −3.6 mm, ML 3.2 mm, 4.6 DV mm), mThal (AP −1.1 mm, ML 0.3 mm, DV −3.2 mm), or mPFC (AP 2.0 mm, ML 0.3 mm, DV −2.9 mm). Either 10 min or 1 month later, a 400um core optical fiber (0.48NA, BFH48-400 ThorLabs) was implanted in the NAc shell at various positions along the rostrocaudal axis (AP 0.9 to 1.8 mm, ML 0.6 mm, DV −4.7 mm).

For the cell body imaging experiments, AAVrg-hSyn1-GCaMP6f-P2A-nls-dTomato (at 1.0 × 10^{13} GC/ml from Addgene – plasmid #51085 – courtesy of Jonathan Ting) was delivered into the rostral or caudal NAc shell (AP 1.7 or 1.0 mm, ML 0.6 mm, DV −4.7 mm). 10 min later, the same 400um core optical fiber was implanted into the BLA, vHipp, or mPFC, 200 um dorsal to the coordinates stated above. Implants were secured with dental cement (Lang) and skull screws (Morris). Behavioral training commenced one to two weeks following surgery.

For the optogenetic experiments, AAV5-CaMKIIa-eArchT3.0-EYFP (at 5.0 × 10^{12} GC/ml from UNC vector core) was delivered into the BLA, vHipp, or mThal at the coordinates detailed above. 10 mins later, a 200um core optical fiber (0.37NA, ThorLabs) was implanted in the rostral or caudal NAc shell (AP 1.5 mm or 1.0 mm, ML 0.6 mm, DV −4.7 mm). These experiments (behavior and brain slice) were conducted 2-3 months after surgery.

Behavioral Testing

Locomotion was assessed in one 30 min visit to an activity box (8.5 × 7 inches) using video tracking software (Ethovision, Noldus; 15 Hz recordings). Transitions between rest and rapid movement were identified using a 'locomotor index' algorithm, which calculates the standard deviation of the animal's position in space over five video frames (Drai et al., 2000; McGinty et al., 2013). We identified conservative thresholds to distinguish periods of rest (< 0.05) and locomotion (> 0.5) that were appropriate for all animals. Transitions to states that were maintained for less than 500 ms were not analyzed.

The operant reward-seeking task was performed in sound attenuating conditioning chambers that had levers available on either side of a centrally located food receptacle (Med Associates). A houselight and speaker were located on the opposite side of the chamber. Mice were placed in these chambers daily for 40 to 60 min. Training consisted of three phases. Initially, a single press on either lever resulted in lever retraction (1 s) and the delivery of 30 μL of sugar water (15% sucrose) to the food receptacle. Mice repeated this stage until they successfully earned and consumed 100 rewards in a single session. During phase two, reward delivery (and the associated 1 s long lever retraction) was contingent on the mice pressing a specific lever (the active lever) while the discriminative stimulus (DS) tone was played (4 kHz, 80 dB, up to 20 s in duration). DS presentations occurred on a variable interval schedule with a mean of 60 s. The DS turned off after either an active lever press or 20 s, whichever came first. Inactive lever presses made at any time and presses on the active lever outside of DS presentations had no consequence during this and the subsequent phase. Mice stayed at this phase until they earned at least 30 rewards in a single session. The third and final phase introduced a non-rewarded stimulus (NS: 2 kHz, 80 dB), which was presented in place of the DS on about half the trials. Both DS and NS presentations during this final phase only lasted 10 s. Lever presses that occurred during NS presentations had no consequence. Once behavioral performance stabilized (typically after 1 month of training across all phases), mice completed several additional training sessions while connected to an optical tether. Fiber photometry recordings of pathway specific fluctuations in GCaMP fluorescence were collected and pooled from two to three subsequent sessions.

The feeding assay associated with the optogenetic experiments was conducted in unfamiliar activity boxes (8.5 × 17 inches), which were bare except for a water bottle that was filled with sweetened chocolate milk (Lactantia). An arduino-based lickometer was used to record consummatory behavior. Total licks were counted as well as number of lick bouts, which were defined as clusters of 3 or more licks without a break greater than 1 s. Mice were placed in this chamber and given free access to the chocolate milk for 60 to 80 min per day. Mice were tethered to optical cables starting with the fourth session and the optogenetic manipulations began on the sixth session. Mice were tested while they had free access to food in their home cage and again shortly after they were placed on food restriction. Test sessions began with a 20 min baseline period, followed by alternating laser Off/On periods, which were each 10 min long. During Laser On periods, approximately 15 mW of 532 nm light (LaserGlow DPSS laser) was directed in the NAc bilaterally.

GCaMP Photometry Recordings

Mice were tethered to a 400 μm core fiber optic patch cord (0.48NA, BFH48-400 ThorLabs) that connected the fiber implant in their head to an optical table and light sensor. The optic table combined light from a 490 nm LED (ThorLabs M490F2, filtered through a 472 nm Semrock bandpass filter) and a 405 nm LED (ThorLabs M405F1, filtered through a 405 nm Semrock bandpass filter) by means of a 458 nm dichroic beam splitter (Semrock FF458-Di02). The intensity of the 472 nm light input into the brain oscillated between 10 and 200 μW at 205 Hz. The 405 nm light input oscillated between 10 and 100 μW at 450 Hz. Both wavelengths of light were directed into the brain via a 488 nm dichroic mirror (Semrock Di02-R488). Light collected from the brain was measured with a 2151 Femtowatt Photoreceiver after it passed through the 488 nm dichroic mirror and was filtered with a 535 nm Semrock bandpass filter (FF01-535/50).

Data were acquired with either the RX-8 signal processor (TDT) or the RZ5P Photometry Processor (TDT). The light signal was sampled at 6 kHz and then demodulated in relation to the 205 and 450 Hz carrier frequencies. The demodulated signals were low-pass filtered (4 Hz). Patch cord autofluorescence resulting from the oscillating 405 nm and 472 nm excitation wavelengths, which was separately measured for each wavelength from untethered patch cords at the end of each testing session, was subtracted from the demodulated signals. The 405 nm control signal was then scaled using a least-squares regression to best fit the 490 nm calcium-sensitive signal in 5 min segments. This scaled 405 nm signal was then subtracted from the 490 nm signal to yield a movement-correct calcium-sensitive signal. The resultant signal was divided by its mean value in 5 min segments to obtain dF/F.

Behavioral event timestamps associated with tones, levers, food port visits, and licks were recorded as digital inputs to the signal processor. Data were extracted, processed, and analyzed using custom MATLAB (Mathworks) scripts. GCaMP fluorescence was aligned to and averaged across specific types of behavioral events, including abrupt changes in locomotion, DS presentations, NS presentations, lever presses, food port entries, and food port exits. Task events were classified further according to the animal's behavior just before or after each event (e.g., cued or uncued lever presses). The first food port visit following each reward delivery was considered to be a consummatory visit, as long as at least 20 licks were made. Non-consummatory food port visits by definition lasted at least 500 ms but had less than 10 licks. Non-consummatory visits that occurred within 5 s of unrewarded lever presses were distinguished from those that were made more than 10 s after any previous lever press or tone presentation.

Brain Slice Electrophysiology

Animals were anesthetized and then perfused with modified artificial cerebrospinal fluid that contained, in mM, 92 NMDG, 20 HEPES, 25 glucose, 30 NaHCO3, 1.25 NaH2PO4, 2.5 KCL, 5 sodium ascorbate, 3 sodium pyruvate, 2 thiourea, 10 MgSO4, 0.5 CaCl2 (pH 7.35). 200 μm thick coronal slices containing the NAc were prepared using a VT-1200 vibratome (Leica) and held at 34°C for 10 min in this same solution. Slices were then transferred to a "holding ACSF" at room temperature, which was identical except that NaCl (92 mM) was included instead of NMDG and the MgSO4 and CaCl2 concentrations were 1 and 2 mM, respectively. The ACSF used on the patch rig was maintained at 31°C and contained, in mM, 119 NaCl, 2.5 KCL, 1.25 NaH2PO4, 2 MgSO4, 2 CaCl2, 24 NaHCO3, and 12.5 glucose. All ACSF preparations were saturated with 95% O2 and 5% CO2. Cells were visualized on an upright microscope with infrared differential interference contrast and fluorescence microscopy. Whole-cell patch-clamp recordings were made using a MultiClamp 700B amplifier using 2 kHz lowpass Bessel filter and 10 kHz digitization with pClamp 11 software (Molecular Devices, Sunnydale, CA). Cells were patched using glass pipets with resistance 4.0-6.0 MΩ, filled with internal solution containing, in mM, 117 cesium methanesulfonate, 20 HEPES, 0.4 EGTA, 2.8 NaCl, 5 TEA-Cl, 4 Mg-ATP and 0.4 Na-GTP (pH 7.3). Spiny neurons identified by morphology, membrane resistance, and hyperpolarized resting membrane potential were patched in the NAc shell in areas with bright eYFP fluorescence. Membrane potential was clamped at −70 mV. Series resistance (10-25 MΩ) and input resistance were measured with 5 mV hyperpolarizing pulses (50 ms). Series resistance remained stable over the period of data collection. EPSCs were evoked in pairs (50 ms interval) with a single stimulating electrode positioned 100-200 μm dorsal to the recorded neuron. Paired pulse ratios were calculated by dividing the amplitude of the second EPSC by the amplitude of the first one. Opsin activation was achieved with 590 nm light (2 mw, ThorLabs, DC4104) directed through the microscope objective.

Retrograde Tracing

Cholera toxin B subunit conjugated to Alexa Fluor (CtB-488, CtB-594; Molecular Probes) was bilaterally injected into the rostral and caudal NAc shell (AP 1.7 or 1.0 mm, ML 0.6 mm, DV −4.7 mm; 0.5μl per side). Animals were sacrificed for analysis 10 days after surgery. 30 μm brain slices were collected from these animals and photographed using with a confocal microscope (Leica TCS SP8, McGill University Cell Imaging and Analysis Network). Fluorescently labeled cells were manually counted using Adobe Photoshop software.

Histology

At the end of each behavioral experiment, animals were anesthetized with 270 mg/kg Euthasol (Merck) and transcardially perfused with 4% paraformaldehyde (PFA, Sigma-Aldrich). Brains were removed, post-fixed in PFA for 24 hr, and then transferred to PBS for 48 hr. Tissue was then sliced into 60um sections on a vibratome (Leica VT1000s) and mounted on microscope slides with a MOWIOL plus DAPI (Sigma Aldrich) solution.

QUANTIFICATION AND STATISTICAL ANALYSIS

Across all statistical tests, $p < 0.05$ was considered significant. Significant interactions with 2-way ANOVAs were followed up with Sidak post hoc tests.

To characterize the heterogeneity of pathway-specific GCaMP fluorescence between animals, we classified each mouse as having Type 1 or Type 2 activity based on the initial direction of the mean signal change following rewarded DS presentations. Specifically, we used the *findchangepts* function in MATLAB to identify abrupt changes in the mean GCaMP signal following rewarded DS presentations, and response type was determined by assessing if the first change was negative (Type 1) or positive (Type 2) relative to the signal mean 5 to 10 s prior to the DS onset.

To identify the onset time of a signal change, we determined the last time point closest to the change point identified with the MATLAB *findchangepts* function when the signal was within 2 standard deviations of baseline. The baseline period used for locomotion was −5 to −3 s and for DS onset was −10 to −5 s.

A subset of the GCaMP6s recordings showed NS associated activity, which was confirmed with paired t tests that compared mean GCaMP6s fluorescence across 5 s windows immediately before and after each NS presentation.

The relationship between food port visit duration and GCaMP6f fluorescence was assessed for each mouse. Pearson's correlation coefficients were obtained using the duration of each food port visit and the corresponding area under the curve in the GCaMP signal. For averaging and statistical comparison, correlation coefficients were transformed using a Fisher's Z-Transformation. A one-sample

t test was used to evaluate if the correlation significantly differed from zero. Average z scores were back-transformed to obtain average Pearson's r values.

To determine how the different components of rewarded trials uniquely contributed to changes in GCaMP fluorescence, we modeled the GCaMP signals as the sum of the discrete changes in fluorescence that best associated with each task event (Parker et al., 2016). A convolution matrix consisting of 1 s and 0 s, with 1 s representing the time interval relative to each behavioral event (−1 to +6 s), was used to identify regression coefficients (response kernels) that minimized the difference between the actual GCaMP signal and the modeled signal. Assuming linearity in the responses to each event, response kernel regression coefficients should characterize how input activity specifically correlates with each type of behavioral event. Signals were modeled by summing of the convolution of each behavioral event timestamp with the response kernel that corresponded to that event (R^2 = 0.21 ± 0.02). The model can be expressed as:

$$g(t) = g_0 + \sum_{t'=-1s}^{2s} a(t-t')k^a(t') + \sum_{t'=-1s}^{2s} b(t-t')k^b(t') + \ldots + error \qquad \text{Equation 1}$$

In this equation, the GCaMP signal is *g(t)*, the time series of each behavioral event (e.g., DS presentation or lever press) correspond to *a, b*, etc., and the response kernels for each event is represented as k^a, k^b, etc. The response kernels were identified using the least-squares method (*glmfit* function in MATLAB).